Philosophical Magazine

ISSN: 1478-6435 (Print) 1478-6443 (Online) Journal homepage: http://www.tandfonline.com/loi/tphm20

Vacancy-like defects in nanocrystalline SnO_2: influence of the annealing treatment under different atmospheres

C. Macchi, M. A. Ponce, P. M. Desimone, C. M. Aldao & A. Somoza

To cite this article: C. Macchi, M. A. Ponce, P. M. Desimone, C. M. Aldao & A. Somoza (2017): Vacancy-like defects in nanocrystalline SnO_2: influence of the annealing treatment under different atmospheres, Philosophical Magazine, DOI: 10.1080/14786435.2017.1415466

To link to this article: https://doi.org/10.1080/14786435.2017.1415466

Published online: 20 Dec 2017.

PHILOSOPHICAL MAGAZINE, 2017
https://doi.org/10.1080/14786435.2017.1415466

Taylor & Francis
Taylor & Francis Group

Vacancy-like defects in nanocrystalline SnO_2: influence of the annealing treatment under different atmospheres

C. Macchi[a#], M. A. Ponce[b#], P. M. Desimone[b#], C. M. Aldao[b#] and A. Somoza[a‡]

[a]CIFICEN (UNCPBA-CICPBA-CONICET) and Instituto de Física de Materiales Tandil – IFIMAT (UNCPBA), Tandil, Argentina; [b]Institute of Materials Science and Technology (INTEMA), University of Mar del Plata and National Research Council (CONICET), Mar del Plata, Argentina

ABSTRACT

The study of electronic and chemical properties of semiconductor oxides is motivated by their several applications. In particular, tin oxide is widely used as a solid state gas sensor material. In this regard, the defect structure has been proposed to be crucial in determining the resulting film conductivity and then its sensitivity. Here, the characteristics of vacancy-like defects in nanocrystalline commercial high-purity tin oxide powders and the influence of the annealing treatment under different atmospheres are presented. Specifically, SnO_2 nanopowders were annealed at 330 °C under three different types of atmospheres: inert (vacuum), oxidative (oxygen) and reductive (hydrogen). The obtained experimental results are discussed in terms of the vacancy-like defects detected, shedding light to the basic conduction mechanisms, which are responsible for gas detection.

ARTICLE HISTORY
Received 18 October 2016
Accepted 5 December 2017

KEYWORDS
Tin oxide; nanocrystals; point defects; positron annihilation; Raman spectroscopy; electrical conductivity

Introduction

Polycrystalline metal oxide semiconductors are widely used for gas sensor and varistors applications. The sensing properties of tin oxide thick films gas sensors are influenced by the microstructural features, such as the grain size of the semiconductor particles, defect concentration and the connectivity between particles [1–3].

Oxygen vacancies in semiconducting oxides act as electron donors and Schottky-type intergranular barriers determine the conductivity of polycrystalline oxide semiconductors [1,4,5]. The relation between the barrier height (ϕ) and the potential barrier width (Λ) is regularly obtained by solving the Poisson's equation under the 'depletion approximation' [6,7]. In this approximation, for a spherical grain of radius R, the barrier height is directly related to the donor density N_d and the potential barrier width as follows [8]:

CONTACT C. Macchi cmacchi@exa.unicen.edu.ar
[#]Consejo Nacional de Investigaciones Científicas y Técnicas (CONICET)
[‡]Comisión de Investigaciones Científicas de la Provincia de Buenos Aires (CICPBA)

$$\phi = \frac{e^2 N_d}{2\varepsilon_0 \varepsilon_r} \Lambda^2 \left[1 - \frac{2\Lambda}{3R}\right] \quad (1)$$

where ε_0 is the vacuum permittivity, ε_r the relative permittivity and e the electron charge.

Despite technological advances, the fundamental understanding on tin oxide gas sensors has improved through the elucidation of the role of Schottky barriers, chemisorbed gases and defects formation [8]. Particular attention has been paid to the understanding of the basic sensing mechanisms involved that depend on the defect formation within the grain and at the surface.

Positron annihilation spectroscopy (PAS) is a well-recognised, non-destructive nuclear technique for studying open volume defects in solids [9]. In particular, PAS has demonstrated to be a powerful tool to investigate the presence of vacancy-like defects in metals and semiconductors [10,11]. In recent years, PAS has been successfully used to obtain information on the defect structure in monocrystalline semiconductor metal oxides as well as in polycrystalline ones [12–18]. Even though defects are expected to directly affect the electrical properties of semiconductors, to our knowledge only few papers were published regarding the use of PAS to investigate nanocrystalline tin oxide [15,16]. For example, Shek et al. [15] used an experimental variant of PAS, Positron Annihilation Lifetime Spectroscopy (PALS) to characterise the interface defects and their evolution with the annealing temperature and time on compacted nanocrystalline SnO_2 powders prepared by the sol–gel route; on the basis of the obtained results, these authors concluded that in the samples studied there were two types of defects: monovacancies and microvoids.

In the present work, electrical measurements were carried out to connect the conductivity of the samples with the defect structure, as it is crucial in determining the gas film sensitivity [19]. With this goal, we studied the influence of the treatment atmosphere on the defect structure of annealed nanocrystalline tin oxide films. The microstructure of the treated samples was characterised by means of scanning electron microscopy (SEM) and X-ray diffraction (DRX). Raman spectroscopy and PALS were used to obtain information about vacancy-like defects into the different tin oxide samples.

The paper is organised as follows: in Section *Experimental*, information about sample preparation, and experimental details on the techniques used are given. In Section *Results and Discussion*, we report and discuss the results obtained using the different experimental techniques; moreover, a general discussion is also presented. Finally, conclusions are summarised.

Experimental

Sample preparation

Commercial high-purity SnO_2 (Aldrich, medium particle size 0.4 μm) was ground until a medium particle size of 0.1 μm. Size particle distributions of the powders

were determined by the Sedigraph technique with a Micromeritics. Powder was thermally treated up to 330 °C for 1 h using a heating rate of 1 °C/min. After heating in an air atmosphere, samples were cooled down up to room temperature (RT): initial powder named P_1. Then, three different thermal treatments were carried out to obtain samples with a different defect structure [20,21]. A fraction of the powder was thermally treated for 4 h in a N_2 with 5% H_2 atmosphere at 330 °C. This powder was labelled P_{H_2}. Another fraction was exposed to dry air (760 mm Hg, 330 °C) during 4 h and was labelled P_{O_2}. Finally, the last fraction of P_1 was thermally treated in vacuum at 330 °C during 4 h; this fraction of powder was labelled P_v. After the thermal treatments, the resulting powders were cooled up to RT and pressure compressed to prepare three pairs of discs to be analysed by means of PALS.

In order to carry out electrical measurements, we prepared tin oxide films using the powders described above. A paste was made using the initial powder mixed with an organic binder (glycerol). The used solid/organic binder ratio was ½, and no dopants were added. Thick, porous film samples were made by painting *(Doctor Blade Technique)* onto insulating alumina substrates with Ti and Pt deposited by sputtering on which electrodes with an interdigitated shape were delineated using laser ablation, see Figure 1 and [21]. After painting, samples were thermally treated for 1 h in air at 100 °C. This treatment was made in order to evaporate the organic binder and to improve the adhesion of the films on the alumina substrates. Later, the films were thermally treated up to 330 °C using a heating rate of 1 °C/min, following the same procedure used to prepare the samples to be measured by PALS. One of the samples was exposed to an air atmosphere at 330 °C for 1 h. After the thermal treatment, this sample was cooled down up to RT (labelled F_{O_2}, film exposed to oxygen atmosphere); then, electrical measurements were carried out at RT. In order to have equivalent samples to those prepared for PALS measurements, the F_{O_2} sample was thermally treated for 4 h in a vacuum atmosphere (10^{-4} mm Hg) and cooled up to RT in the same atmosphere (F_v). After this treatment, electrical measurements were carried out in vacuum. Finally, the film was treated as the powder P_{H_2}; that is, in a N_2 with 5% H_2 atmosphere at 330 °C to avoid metallisation. This film was cooled up to RT and labelled F_{H_2}; then the film resistance was measured. The treatments applied to the films were the same as those used to treat the shaped-disc samples. In short, subscript O_2 refers to powders and films treated in an oxygen atmosphere, subscript V refers to powders and films treated under vacuum, and subscript H_2 refers to powders and films treated with hydrogen. Table 1 facilitates the quick reference to the kind of samples and treatments used.

Microstructural characterisation

A JEOL JSM 6460-S scanning electron microscope was employed to analyse the surfaces and cross sections of the tin oxide films. X-ray diffraction and Raman

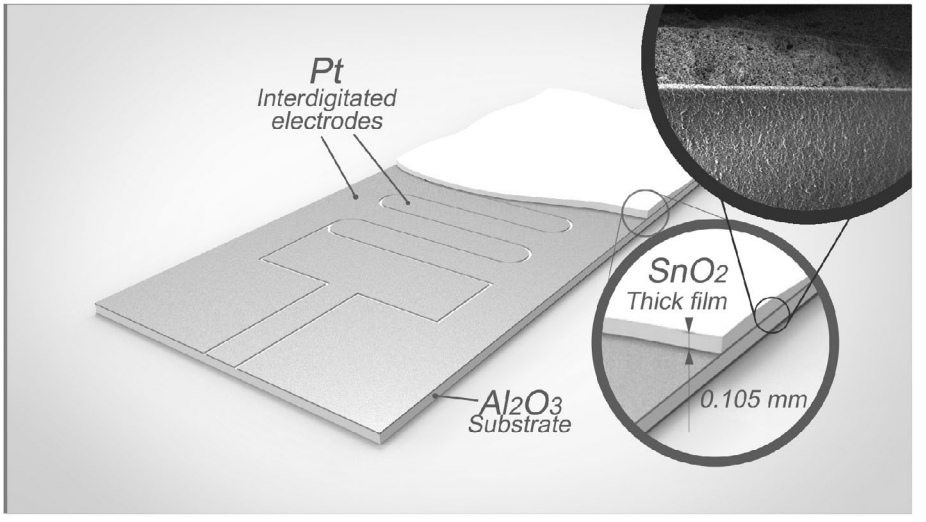

Figure 1. Substrate of 20 mm length and 10 mm wide used to carry out electrical measurements. On the insulating alumina, Ti and Pt deposited by sputtering and then electrodes with an interdigitated shape were delineated using laser ablation. For measurements, external contacts were directly carried out on the metallic electrodes of the substrate. To observe these details, the tin oxide film is partially depicted.

Table 1. Powders and films treatment at different atmospheres. P_1 is the original commercial powder, O_2 corresponds to the samples treated in oxygen atmosphere at 330 °C during 4 h, *v* corresponds to samples treated under vacuum at 330 °C during 4 h, and H_2 corresponds to samples treated for 4 h in a N_2 with 5% H_2 atmosphere at 330 °C.

P (powder)	*F* (film)	Treatment
P_1	–	Original commercial powder
P_{O_2}	F_{O_2}	Oxygen atmosphere at 330 °C during 4 h
P_v	F_v	Under vacuum at 330 °C during 4 h
P_{H_2}	F_{H_2}	Hydrogen atmosphere at 330 °C during 4 h

were used to analyze the superficial and bulk changes after the thermal treatments under different atmospheres. XRD patterns were obtained using a PANalytical X′Pert PRO diffraction system employing the CuKα radiation (λ = 0.1542 nm) at 40 kV as generator voltage and 40 mA as generator current. The samples were scanned between 20° and 80° with a step size of 0.02°. The XRD data were analysed using X′Pert PRO HighScore software, and the crystallographic data for each phase were taken from the literature [22]. Finally, to gain confidence in the quality of the films, Raman spectra were also recorded. Raman spectra were acquired at RT with a Renishaw in via Reflex micro-spectrometer equipped with a charge-coupled device (CCD) detector of 1024 × 256 pixels. An Ar laser line (514 nm, 50 mW) was used as the excitation source in combination with a grating of 2400 grooves/mm. A 50× (0.75NA) Leica metallurgical objective was used in the excitation and collection paths. A neutral density filter was used to reduce

the incident laser power on the sample to values by about 0.2 mW, as measured with a silicon photodiode (Coherent Inc.). The presence of the binder should be detected in the 1000–2000 cm^{-1} wave number range of the Raman spectra. After the thermal treatments, no traces of the binder were found and the films presented the same spectra as those obtained for the original powder. This result indicates that the purity of the films does not change. In a previous work, by means of XPS, it was checked that this kind of treatment does not contaminate the samples [23].

PALS measurements

PALS spectra were obtained using a fast-fast spectrometer, with a time resolution of 210 ps, in a collinear geometry. As positron source, a 10 μCi sealed source of ^{22}NaCl deposited onto two thin kapton foils (7.5 μm thick) sandwiched between two identical samples was used. The spectra were acquired at RT and, typically 1.5–2 × 10^6 counts per spectrum were collected. The lifetime values reported in this work for each sample are at least an average of ten measurements, at the same experimental conditions. After subtracting the background and the source contribution, positron lifetime spectra were analysed using the POSITRONFIT code [24] As a result, several lifetime components were obtained; each of them is characterised by a lifetime (τ_i) and an associated intensity (I_i), which corresponds to the formation probability of that particular positron state. Such state can be the delocalised one in the crystal lattice (bulk state) or a localised state at a defect site. A general panorama about the meaning of the parameters τ_i and I_i obtained from the decomposition of PALS spectra are given in [25]. In the analysis of PALS spectra, the most statistically robust parameter is the positron mean lifetime $\bar{\tau}$, defined as the sum of the individual lifetimes weighed with the normalised intensity of each lifetime component:

$$\bar{\tau} = \sum_i I_i \tau_i. \tag{2}$$

The increase of $\bar{\tau}$ above the positron lifetime characterising the bulk state (τ_b) indicates that defects are present in the sample [9].

Electrical measurements

The electrical resistances of the films F_{O_2}, F_v and F_{H_2}, subjected to the different gas treatments, were measured after decreasing the temperature from that of the treatment to RT, at a rate of ~5 °C/min in the same atmosphere. For the electrical resistance measurements, an Agilent 34401A multimeter was used. Measurements can directly be compared since the fabrication procedure used allows to produce very reproducible substrates and films (see [21]).

Results and discussion

Microstructure

Figure 2(a) and (b) show typical SEM images of the films studied. The grain size was measured because it is crucial for the electrical properties, as discussed in detail in [26,27]. From the images, the average particle size of the powder and films samples labelled P_1, P_{H_2} and P_{O_2} was determined to be about 80 nm. The average grain size of the sample P_1 was also calculated using the Scherrer formula, yielding values between 65 and 120 nm. These values are in good agreement with those obtained from the SEM images. In the case of films, their average thickness was

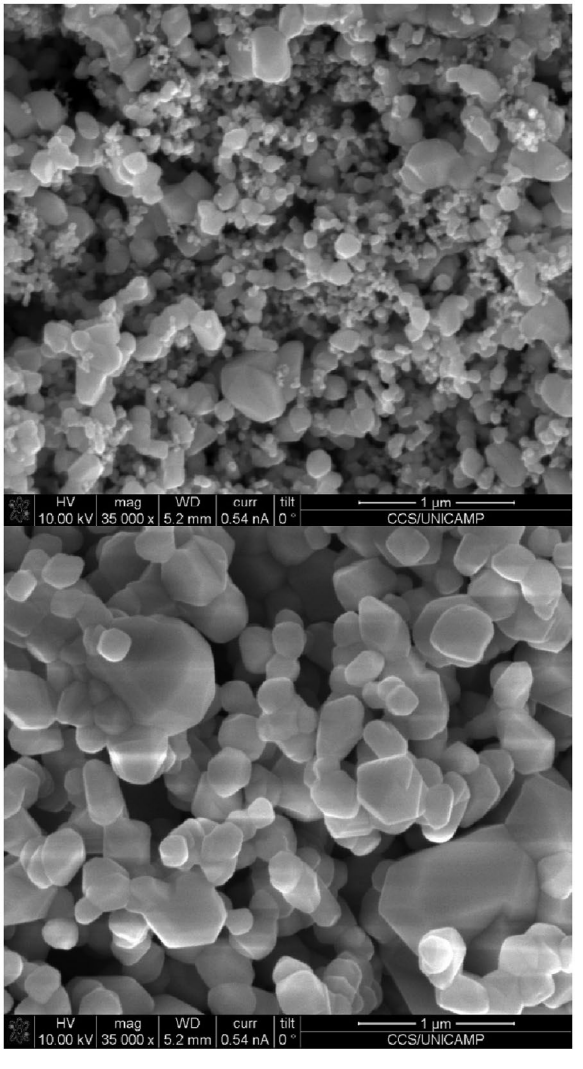

Figure 2. SEM images showing a porous structure of the conformed films: (a) average grain size of 80 nm, and (b) average grain size of 250 nm.

0.105 mm as determined from SEM images of their respective cross sections using a Surtronic 3+(Taylor Hobson) profilometer with a diamond stylus (radius: 1 μm).

Figure 3(a) and (b) show the XRD patterns for the film samples F_{O_2} and F_{H_2}. After the heat treatment under the mentioned atmospheres, the phase of both samples corresponds to the diffraction planes typical of the SnO_2 cassiterite phase (PDF n° 01-071-0652). Therefore, this result indicates that the exposure of the films to a reducing atmosphere at 330 °C does not modify its crystal structure. It can also be observed that the intensities of the X-ray diffraction patterns obtained for F_{O_2} and F_{H_2} samples are similar. Lattice parameters were determined, their values were a = 4.74 Å and c = 3.18 Å, respectively.

Raman spectroscopy results

In nanostructured materials a drastic increase in superficial atoms is observed; that is, atoms which are to some extent affected by the presence of a surface in

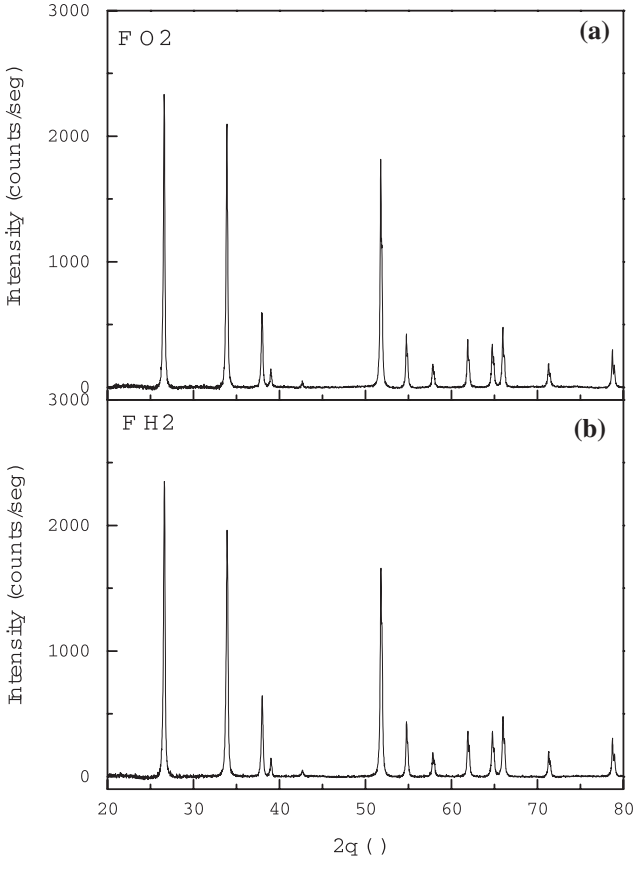

Figure 3. XRD patterns for the SnO_2 film with a grain size of 80 nm. (a) Sample thermally treated at 330 °C in a dry air atmosphere up to 330 °C (initial characterisation), and (b) Sample thermally treated at 330 °C in a N_2 atmosphere with 5% H_2.

their neighbourhood. As a consequence of different environments, the properties of the surface atoms (and specially their vibrational properties) are different; these phenomena can be studied by means of Raman spectroscopy. Moreover, surfaces have a strong tendency to react with the surrounding atmosphere, and the observation of these reaction products is possible to reveal using the micro-Raman technique when the surface fraction inside the focus volume of the microscope objective is important enough [28].

Figure 4(a) shows the Raman spectrum for the heat-treated F_{O_2} sample. This spectrum shows the characteristic bands of SnO_2. The peaks observed at 475, 632 and 775 cm^{-1} have been assigned to the E_g, A_{1g} and B_{2g} vibrational modes of SnO_2 in the F_{O_2} tetragonal rutile structure, respectively [29,30]. In this spectrum, other two peaks appear at 542 and 693 cm^{-1} which are not usually observed in bulk SnO_2. These peaks were related to characteristic modes arising from either vacant sites or a local lattice disorder [31,32]. In Figure 4(b), the spectrum obtained for the F_{H_2} sample is shown. When comparing this spectrum with that obtained for the F_{O_2} sample, a decrease in the overall intensity of the peaks associated with SnO_2 is observed. Pagnier et al. [28] indicated that the surfaces modes observed

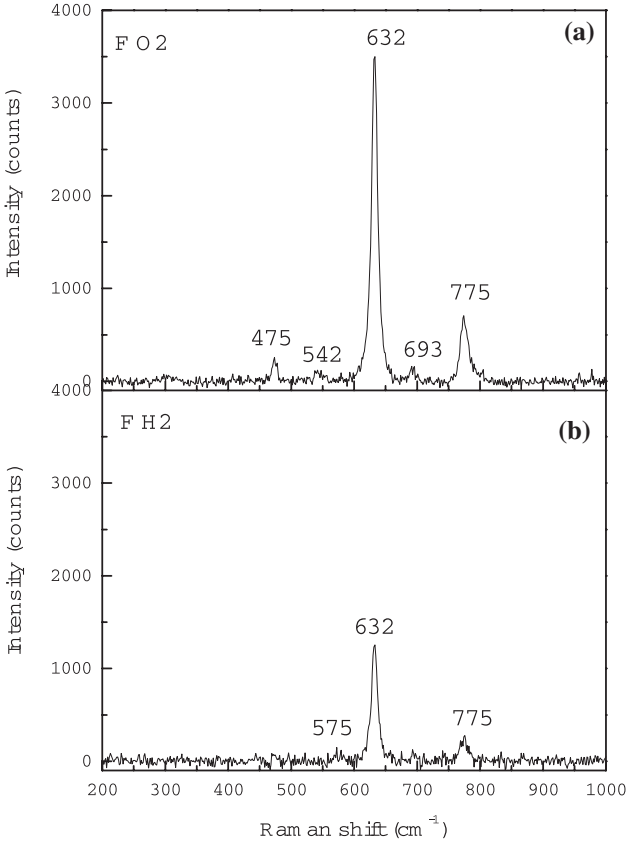

Figure 4. Raman spectra for the heat-treated F_{O_2} film (a) and for the film exposed to a reductive atmosphere of N_2 with 5% H_2 (b).

between 400 and 800 cm^{-1} come from the surface of the grains which are in direct contact with the atmosphere, and not from the whole surface of the grains. It must be mentioned that no chemical changes were observed neither by XRD nor Raman spectroscopy. Moreover, intensities in the XRD patterns showed no changes when the samples were exposed to different atmospheres. This is because X-ray diffraction patterns give information on bulk properties of the materials.

On the other hand, the general decrease in the intensity of the peaks of the Raman spectra corresponding to the F_{H_2} and F_{O_2} samples, respectively, could be explained considering that the technique gives information on superficial changes of the grains. This could be due to a roughness change after hydrogen exposure [33,34], but the film roughness of our samples is very reproducible [21]. Note that as the density of oxygen vacancies (donors) increases, the depletion regions of the grains are narrower and then the Raman intensities decrease [35,36]. Then, the observed results would be an indication that there is a higher number of defects at the F_{H_2} sample than that of the F_{O_2} one.

As can also be seen in Figure 4(b), the peak at 542 cm^{-1} appears shifted towards higher wavenumbers (575 cm^{-1}). This peak has not been previously observed in the Raman spectra of single-crystal or polycrystalline SnO_2 and it was only reported for SnO_2 samples with nanometer grain sizes [37,38]. Sharygin and Vovk [39] suggested that the wide band at ~580 cm^{-1} is not only due to the surface modes, but also to the possible presence of an hydrated tin dioxide $Sn(OH)_4$ (defined as $SnO_2.2H_2O$ as well). Xu et al. [38] assigned this mode to surface defects in SnO_2 nanocrystals, specifically oxygen-related defects. In order to compare the change of the relative intensities of the peaks at 542 and 575 cm^{-1}, the respective intensities of both peaks were normalised to that located at 632 cm^{-1}. In such a way, relative intensities of 0.03 and 0.07, respectively, were obtained. As can also be seen in Figure 4(b), the intensity of the peak located at 575 cm^{-1} increases when the film is exposed to a reductive atmosphere. This behaviour also indicates that the hydrogen reductive atmosphere favours the formation of higher concentration of defects than that formed in the films heat treated in the oxidative atmosphere.

Positron annihilation lifetime spectroscopy results

In all the compacted samples studied, PALS spectra were satisfactorily fitted considering three lifetime components (in all cases χ^2 values vary between 1 and 1.1). Initially, a free constraint fitting analysis of the spectra showed the presence of two almost constant lifetimes $\tau_2 = 350 \pm 5$ and $\tau_3 = 2100 \pm 100$ ps. Then, using a usual procedure to analyse PALS spectra [40], a second analysis was carried out fixing these lifetimes at 350 and 2100 ps, respectively. The second lifetime component makes it possible to identify the kind of open volume defect in which positrons become trapped through the τ_2 value and its respective concentration given by the I_2 value [40].

For all the samples studied in the present work, it was found that the intensity I_3 associated with the long-lived positron lifetime corresponding to the ortho-Positronium annihilation via the pickoff process ($\tau_3 \equiv \tau_0 - P_s$) is lower than 2%. This result indicates that the powder compression process used to fabricate the samples is good enough to produce well-compacted samples with a structure equivalent to a solid material. This assertion is based on the fact that from the analysis the PALS spectra obtained measuring massive samples a long-lived lifetime component with intensity lower than 2% is usually revealed [24].

As a reference sample giving the positron lifetime characteristic of the SnO_2 bulk state (τ_b), well-annealed sintered polycrystalline pure SnO_2 ceramics were measured. In Table 2, values of the characteristic parameters from the decomposition of PALS spectra are reported. Due to the small contribution of the o-Ps component, it was not considered to calculate the mean positron lifetimes ($\bar{\tau}$).

The values of the positron lifetime components presented in the table are in good agreement with those reported for other compacted nanocrystalline oxide powders [15–17] and nanostructured metallic samples [41–43].

Analysing the $\bar{\tau}$ values for all the samples studied, it can be seen that, within the error bars, there are appreciable differences among them. In several metallic-based and nanocrystalline oxides samples, typical values for the second lifetime component between 300 and 450 ps were reported. These τ_2 values were attributed to positron annihilations in defects with an open volume size formed by few vacancies; that is, vacancy clusters [15–17]. On this basis, from the τ_2 values obtained for the SnO_2 samples studied in this work it is reasonable to assume that our samples contain vacancy clusters formed by Sn and O vacancies.

On the other hand, values of the short-lived lifetime (τ_1) are systematically slightly higher than τ_b. This result is compatible with positron annihilations in a mixed state; that is, to τ_1 contributes the reduced bulk lifetime and positron annihilations into small open volume defects with a typical size of a mono or divacancies [9]. Also, a reduction of the τ_1 value can be associated with a decrease in the vacancy-like concentration. In the case of the present work, since in semiconductor oxides isolated oxygen vacancies are not effective positron traps at RT [7–9], vacancy-like defects should be tin-based vacancies.

Table 2. Characteristic positron lifetimes and their associated intensities (I_1 (%) = 100 − I_2) obtained from the decomposition of PALS spectra. represents the positron mean lifetime (see text). (*F*) indicates that the corresponding lifetime value was fixed for a further analysis of the PALS spectra. Detailed information on the different thermal treatments is given in the item Sample preparation of Section EXPERIMENTAL.

Sample	τ_1 (ps)	τ_2 (ps)	I_2 (%)	$\bar{\tau}$ (ps)
Sintered SnO_2 annealed sample	166 ± 1	–	–	–
P_1	170.5 ± 0.5	350 (*F*)	22.1 ± 0.5	210.2 ± 0.5
P_{vac}	174.4 ± 0.5	350 (*F*)	19.3 ± 0.5	208.3 ± 0.5
P_{H_2}	169.1 ± 0.5	350 (*F*)	30.0 ± 0.5	223.4 ± 0.5
P_{O_2}	172.5 ± 0.5	350 (*F*)	22.8 ± 0.5	213.0 ± 0.5

Identical τ_2 values indicate that positrons are annihilating in the same kind of vacancy cluster (see [9,10]). However, the intensities I_2 associated with the second lifetime component depend on the atmosphere under which the thermal treatments were carried out. The I_2 value obtained for the sample treated in vacuum is lower than those corresponding to the samples treated under non-inert atmospheres. Taking as a reference the sample treated in vacuum, it can be concluded that the reductive atmosphere (H_2) favours the formation of a higher concentration of vacancy clusters with respect to that of the sample treated in the oxidative atmosphere (O_2). The results obtained by PALS show the same trend as those obtained by Raman spectroscopy, indicating that both techniques provide the same nanostructural information as the SnO_2 samples studied.

In polycrystalline materials, positron trapping depends on the size of the open volume at atomic scale associated with the positron trap, mainly vacancy-like defects, dislocations, voids and grain boundaries. Positron trapping is governed by two different regimes: transition-limited and diffusion-limited. Each positron trapping regime is dependent on the grain size of the polycrystal and the positron diffusion length in the material (L_+). Typical L_+ values for metals and semiconductors are around one hundred nanometers. For grain sizes lower than L_+, the dominant positron trapping regime is the transition-limited one. On the contrary, diffusion-limited regime governs positron trapping for grain sizes higher than L_+ [44].

To evaluate the intragrain (i.e. defects inside the grain) and intergrain (i.e. defects in grain boundaries) positron trapping in SnO_2 nanopowder samples submitted to the same thermal treatments in the non-inert atmospheres with two different average grain sizes were measured. Specifically, the first set of samples was the same measured previously (see results for P_{H_2} and P_{O_2} in Table 2). The second set of samples was the same SnO_2 nanopowders, but with a bigger grain size (250 nm). This grain size was obtained applying to the samples a thermal treatment in nitrogen atmosphere at 1300 °C for 2 h.

Values of the positron parameters obtained from the measurements on both kind of samples are reported in Table 3. As can be seen in the table, for each set of samples the mean positron lifetime systematically decreases for increasing grain sizes. This behaviour, independently of the treatment atmosphere, means that bigger grains contain a lower concentration of defects. Moreover, the constancy of τ_2 values indicates that the same kind of vacancy clusters is present in

Table 3. Characteristic positron lifetimes and their associated intensities (I_1 (%) = 100 − I2) obtained from the decomposition of the PALS spectra for a set of samples treated under two different atmospheres and grain sizes.

Sample	Grain size (nm)	τ_1 (ps)	τ_2 (ps)	I_2 (%)	$\bar{\tau}$ (ps)
H_2 @ 330 °C	80	169.1 ± 0.5	350 (*F*)	30.0 ± 0.5	223.4 ± 0.5
O_2 @ 330 °C	80	172.5 ± 0.5	350 (*F*)	22.8 ± 0.5	213.0 ± 0.5
H_2 @ 330 °C	250	170.9 ± 0.5	350 (*F*)	23.9 ± 0.5	216.2 ± 0.5
O_2 @ 330 °C	250	175.4 ± 0.5	350 (*F*)	14.6 ± 0.5	202.3 ± 0.5

both sets of samples. Conversely, I_2 values decrease when the grain sizes increase. According to the literature, vacancy clusters in nanopowder materials are expected to be localised in the intersections of two or more grain boundaries [15,17]. In such a way, the results described in the previous paragraphs are consistent with the presence of vacancy-like defects located at the grain boundaries. For larger grains, a lower fraction of positrons are annihilated at the grain boundaries; that is, a lower amount of positrons become trapped in this kind of defect.

On the other hand, when the grain size increases, a slight increment of τ_1 is observed. Using the same arguments when discussing the results reported in Table 2, the τ_1 behaviour can be interpreted as that a higher number of positrons are annihilating in tin-based vacancies located inside the grains.

Summarising, based on PALS results it can be concluded that, in both sets of samples with two different grain sizes and treatment atmospheres, the contribution to the positron signal comes from a competitive annihilation process between positrons trapped at vacancy clusters formed by Sn and O vacancies located at the grain boundaries or intragranular defects with a typical size of a Sn monovacancy or a Sn–O (or Sn–Sn) divacancy.

Electrical measurement results

As reported in Table 4, different conductivities were measured for the F_{O_2}, F_v and F_{H_2} films. In particular, there is an increase in the conductivity for the film treated under a reductive atmosphere. This behaviour indicates lower and narrower potential barriers for the hydrogen-treated samples.

General discussion

Tin oxide is a wide band-gap (3.6 eV) semiconductor of *n*-type due to oxygen deficiency. Indeed, O vacancies are the dominant defects in this kind of materials and they behave as donor impurities [5]. In previous works, we assumed that oxygen chemisorbs at the grain surface, increasing the height and width of the intergrain barriers [45–47]. However, from electrical measurements we can deduce that, at high enough temperatures, oxygen diffuses in/out-to the grains (depending on the treatment atmosphere), annihilating oxygen vacancies (when samples are treated in a rich dry air atmosphere) and thus reducing the donor concentration. In the literature, from electron spin resonance (ESR) measurements,

Table 4. Electrical film resistance for the film thermally treated at different gas atmospheres. Given the geometry of our films, the conductivity in S/m is $\sigma \approx 9.4/R$.

Film treatment	Resistance (kΩ)
F_{vac} (vacuum)	2.5
F_{O_2} (oxygen)	61000
F_{H_2} (hydrogen)	0.195

it has been proposed that the adsorbed oxygen can ionise to various O anion species when electrons from SnO_2 can be transferred to the chemisorbed oxygen [48–53]. Those O vacancies changes were also observed by means of the infrared spectroscopy (IR). By detecting the second ionisation of oxygen vacancies inside the grains, changes in the band bending could be determined [54]. For the sake of simplicity, in this work we will consider that the main adsorbed oxygen species on SnO_2 surface is O^-_{ads}.

The oxygen exchange equilibrium between SnO_2 with the gas phase is regularly written as [55]:

$$O_{latt} \Leftrightarrow 1/2O_2 + V_0^{++} + 2e^- \tag{3}$$

where O_{latt} is a neutral oxygen at the crystal, $V_O{}^{++}$ is a doubly ionised oxygen vacancy, e^- is an electron and O_2 an oxygen molecule at the gas phase. Equation (3) implies several mechanisms for oxygen transport from the crystal to the gas phase and *vice versa*, which were explained in previous works [2,5,46,56]. This reaction is in equilibrium and the concentrations of the species involved depend on the partial O pressure present in the gas phase. When SnO_2 films are exposed to vacuum, the surface oxygen desorption improves the sample conductivity. Also, O migrates from the bulk to the surface increasing the oxygen vacancies (Equation (3) moves to the right). Sadek et al. [57] stated that when tin oxide is exposed to H, it reacts with the chemisorbed O and produces H_2O, which is expressed in Equation (4):

$$H_2 + O^{2-}_{(ads)} \rightarrow H_2O_{(g)} + 2e^-. \tag{4}$$

This reaction takes place at the surface of the material, and it does not imply any change in the chemical composition of the metal oxide. In a previous work, the same kind of samples was treated in an H_2 atmosphere at higher temperatures (450 °C); in such a case, the presence of metallic tin was detected, as reported in [58]. Conversely, in the present work, only surface oxygen reacts with hydrogen leaving the surface and then the sample conductivity increases as reported in Table 4. Even though O migration increases the oxygen vacancy concentration, grains are far from metallisation, which are reflected from the XRD patterns and electrical conductance measurements.

The surface and bulk phenomena described above have direct effects on the band structure at the intergrains and then on the electrical properties of the polycrystals which are schematically depicted in Figure 5. In this figure, we have plotted two nanograins in contact showing the top of the valence band (E_V) and the bottom of the conduction band (E_C) along the grains. These two bands were sketched for each atmosphere used to thermally treat the tin oxide samples. The Fermi level position within the band gap should reflect the observed conductivities due to exposures to the non-inert and inert atmospheres. In such a case, the Schottky barriers are expected to be small for the samples exposed to hydrogen

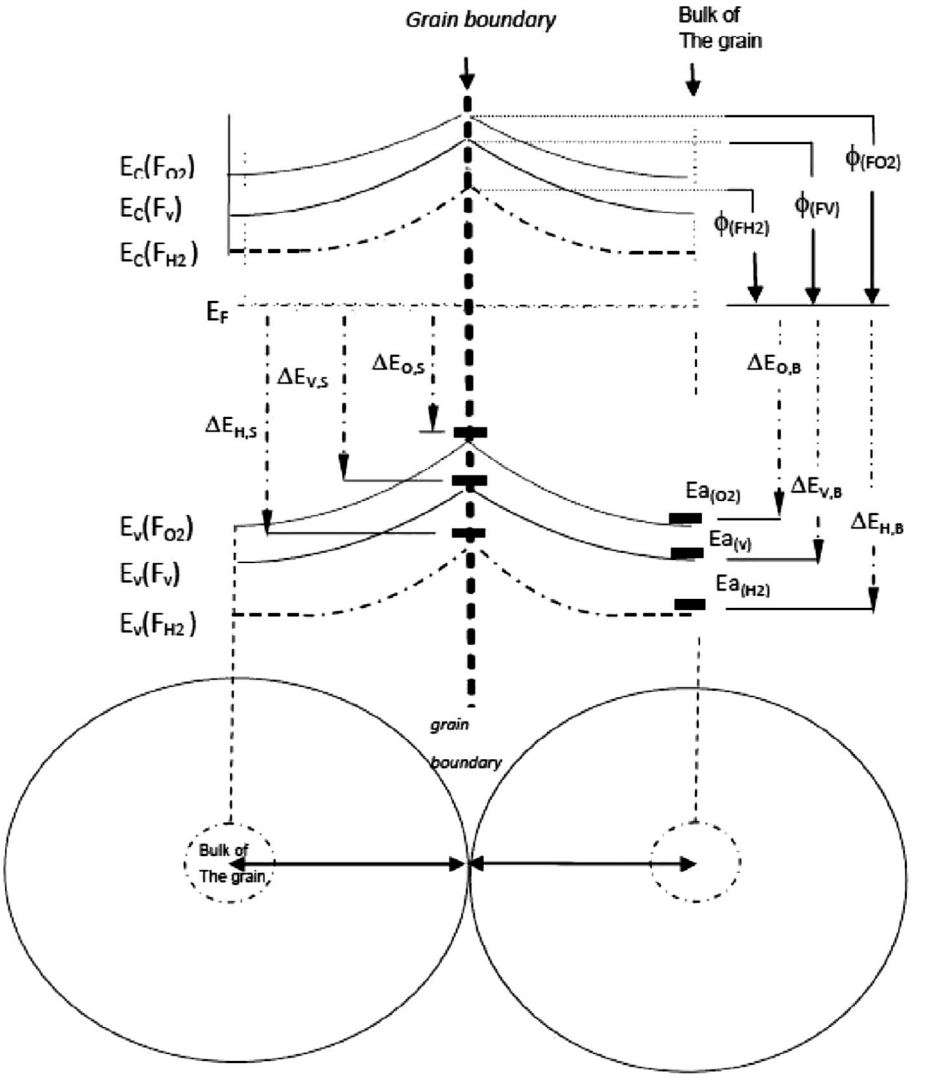

Figure 5. Energy gains ($E_F - E_a$) after an electron transfer from the reservoir (the Fermi level) to the acceptor level (E_a) at the centre and at the surface of a grain. In this plot, energy gains are presented for the samples heat treated in three different atmospheres (see text).

and high for those treated under vacuum; while for samples treated under the oxygen atmosphere the Schottky barrier should be the highest one. This barrier behaviour has been regularly reported for oxidising and reducing gases [59,60]. Also, our electrical measurements indicate that for samples treated in O inside the grain there is a low donor concentration. Hence, the Fermi level should be deep in the band gap along the whole grain.

The concentration of charged point defects changes radically with the Fermi level position [61]. Indeed, this prevents doping of a given type in many cases; and in particular, for wide band gap semiconductors [62]. In Figure 5, the origin of

this dependence for an acceptor point defect is shown. The point defect formation energy of a neutral empty acceptor does not depend on E_F. Conversely, when an acceptor level E_a (which is below the Fermi level) is occupied, the electron transfer leads to an energy gain $\Delta E = E_F - E_a$. Therefore, the formation energy of an ionised acceptor decreases with the Fermi level position or similarly increases with the intergranular barrier height (ϕ). In Figure 4, we have also represented the energy gains at the surface and inside the bulk of the grains (i.e. the intragranular regions) after an electron transfer from the reservoir (the Fermi level) to the acceptor level. Conductivity measurements point out that for the oxidative atmosphere, at the surface and inside the bulk of the grains, the energy gains $\Delta E_{O,S}$ and $\Delta E_{O,B}$, respectively, for the sample P_{O_2} (and F_{O_2}) are smaller than those for the samples P_v (and F_v) and P_{H_2} (and F_{H_2}).

In this scenario, it could be assumed that samples thermally treated under an oxygen atmosphere should have a lower tin-based vacancy concentration than those obtained for samples treated under vacuum or hydrogen. This behaviour should be reflected in changes of the short-lived positron lifetime (see Table 2). However, in the case of the sample treated in hydrogen the decrease in the tin-based vacancy concentration inside the grain, inferred from the reduction of τ_1, is not consistent with the above-mentioned assumption. This inconsistency on the interpretation of the results obtained could be solved considering that the formation energy not only depends on the Fermi level position, but on the atomic chemical potentials [57]. For example, as the oxygen atomic chemical potential directly depends on its partial pressure under oxygen-rich conditions, vacancy-like defects involving oxygen deficiency increase their formation energy. On the contrary, those defects involving oxygen excess will be easily formed. Therefore, the formation energy of a tin-based vacancy reduces under oxygen-rich conditions.

The interplay between the Fermi level position and the chemical potential for charged acceptor defects is summarised in the scheme presented in Figure 6. In this figure, we present a graphical description in which the apparent inconsistency between electrical measurements and PALS results is solved. The three solid lines would represent the tin-based vacancy formation energy as a function of the Fermi level position with respect to the acceptor level and for the three different treatment atmospheres. Note that the ΔE plotted in this figure are those depicted in Figure 5.

In the sketch of Figure 6, the empty circles indicate vacancy formation energies at the near surface region of the grains while the filled circles represent the vacancy formation energies inside the grains. Note that a low vacancy formation energy implies, for any species, a higher point defect concentration. Thus, the observed trends (see the arrow sequences) for the tin-based vacancy concentration at the surface and in the bulk of the grains are in good agreement with the dependence of the vacancy formation energy with the Fermi level position. Specifically, the tin-based vacancy concentration at the near surface region of the

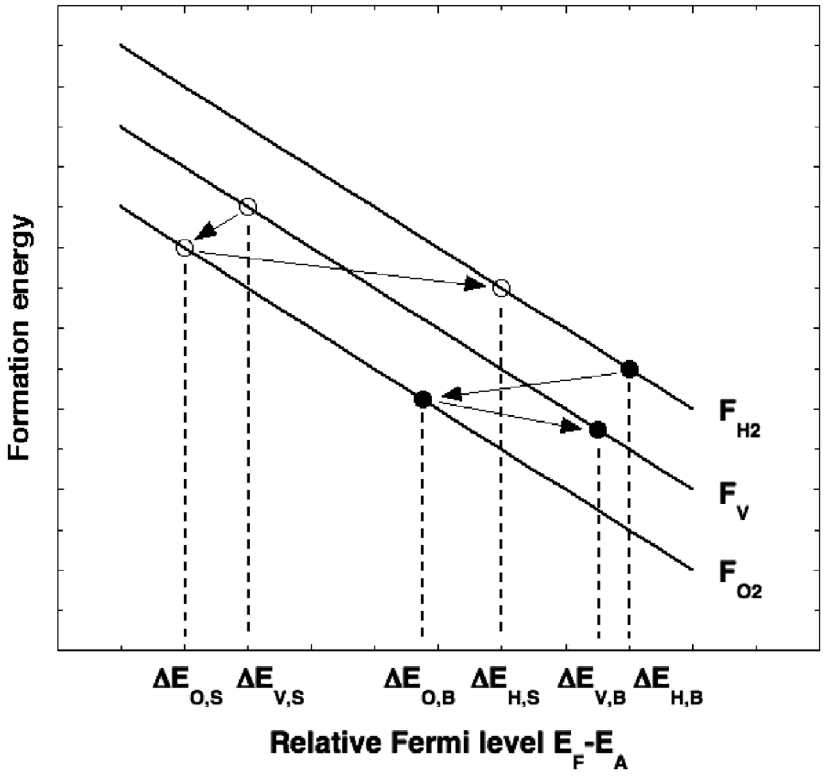

Figure 6. Schematic representation describing the tin-based vacancy formation energy as a function of the Fermi level position (E_F) with respect to the acceptor level (E_A). Each solid line represents the thermal treatments carried out under different atmospheres: vacuum (F_v), hydrogen (F_{H_2}) and oxygen (F_{O_2}). Empty circles indicate the formation energies at the near surface region of the grains while filled circles are the formation energies inside the grains. Arrows indicate the sequence for the decrease in the formation energy and, therefore, the increase in the defect concentration.

grains systematically increases depending on the following atmosphere sequence in which SnO_2 samples were thermally treated: that is, vacuum → O → H. On the other hand, vacancy concentration inside the grains systematically increases when the treatment atmosphere sequences is: H → O → vacuum.

Conclusions

The results obtained studying samples of nanocrystalline commercial high-purity tin oxide powders thermally treated under non-inert and inert atmospheres can be summarised as follows:

- Relatively mild thermal treatments not only affect the surface of the nano-grains, but the defect concentrations in the bulk.
- In all samples, two types of vacancy-like defects were detected: (i) At the surface of the grains, vacancy clusters formed by Sn and O vacancies; and

(ii) Inside the grains, Sn-based vacancies associated with small open volumes (typically, mono- or di-vacancies).

- The interplay between the Fermi level position and the chemical potential determines the charged acceptor defects concentration. This concentration depends on the region of the grains and the treatment atmosphere. In particular, (i) At the surface of the grains, concentration increases according to the atmosphere sequence vacuum → oxygen → hydrogen; and (ii) Inside the grains, defect concentration increases according to the atmosphere sequence oxygen → hydrogen → vacuum.
- Treatments under the reductive atmosphere (i.e. H_2) result in the highest conductivity. In this case, the highest concentration of vacancy clusters at the surface of the grains and the lowest concentration of Sn-based vacancies were found. Results indicate that potential barriers are lower and narrower for the hydrogen-treated samples.

Acknowledgements

M.A.P. and C.M.A. wish to thank Mr Nicolás Tibaldi for his technical assistance.

Disclosure statement

No potential conflict of interest was reported by the authors.

Funding

This work was supported by the Agencia Nacional de Promoción Científica y Tecnológica (Argentina) [grant number PICT 2015-1832] and [grant number PICT 2012-1806]; Consejo Nacional de Investigaciones Científicas y Técnicas (Argentina) [grant number PIP #114-201101-00151]; Comisión de Investigaciones Científicas de la Provincia de Buenos Aires – CICPBA (Argentina); and Universidad Nacional del Centro de la Provincia de Buenos Aires – UNCPBA (Argentina).

References

[1] M.J. Madou and R. Morrison (eds.), *Chemical Sensing With Solid State Devices*, Academic Press, San Diego, CA, 1989.
[2] M.A. Ponce, C.M. Aldao, and M.S. Castro, *Influence of particle size on the conductance of SnO_2 thick films*, J. Eur. Ceram. Soc. 23 (2003), pp. 2105–2111.
[3] X. Wang, S.S. Yee, and W.P. Carey, *Transition between neck-controlled and grain-boundary-controlled sensitivity of metal-oxide gas sensors*, Sens. Actuators B, Chem. 25 (1995), pp. 454–457.
[4] N. Barsan and U. Weimar, *Conduction model of metal oxide gas sensors*, J. Electroceram. 7 (2001), pp. 143–167.
[5] M. Batzill and U. Diebold, *The surface and materials science of tin oxide*, Prog. Surf. Sci. 79 (2005), pp. 47–154.

[6] S.M. Sze (ed.), *Physics of Semiconductor Devices*, Wiley, New York, NY, 1981.
[7] K. Kao (ed.), *Dielectric Phenomena in Solids*, Elsevier Academic Press, San Diego, CA, 2004.
[8] C. Malagù, V. Guidi, M.C. Carotta, and G. Martinelli, *Unpinning of Fermi level in nanocrystalline semiconductors*, Appl. Phys. Lett. 84 (2004), pp. 4158–4160.
[9] P. Hautojärvi and C. Corbel, *Positron spectroscopy of defects in metals and semiconductors*, in *Positron Spectroscopy of Solids, International School of Physics «Enrico Fermi», Course CXXV*, A. Dupasquier and A.P. Mills Jr., eds., IOS Press, Amsterdam, 1995, p. 491.
[10] R. Krause-Rehberg and H.S. Leipner (eds.), *Positron Annihilation in Semiconductors: (Defect Studies, Springer Series in Solid State Science)*, Springer, Berlin, 1999.
[11] F. Tuomisto and I. Makkonen, *Defect identification in semiconductors with positron annihilation: Experiment and theory*, Rev. Mod. Phys. 85 (2013), pp. 1583–1631.
[12] F. Tuomisto, V. Ranki, K. Saarinen, and D.C. Look, *Evidence of the Zn vacancy acting as the dominant acceptor in n-type ZnO*, Phys. Rev. Lett. 91 (2003), pp. 205502:1–4
[13] I. Makkonen, E. Korhonen, V. Prozheeva, and F. Tuomisto, *Identification of vacancy defect complexes in transparent semiconducting oxides ZnO, In_2O_3 and SnO_2*, J. Phys.: Condensed Matter 28 (2016), pp. 224002:1–7.
[14] G. Brauer, W. Anwand, W. Skorupa, J. Kuriplach, O. Melikhova, C. Moisson, H. von Wenckstern, H. Schmidt, M. Lorenz, and M Grundmann, *Defects in virgin and N+-implanted ZnO single crystals studied by positron annihilation, Hall effect, and deep-level transient spectroscopy*, Phys. Rev. B. 74 (2006), pp. 045208:1–10
[15] C.H. Shek, J.K.L. Lai, and G.M. Lin, *Investigation of interface defects in nanocrystalline SnO_2 by positron annihilation*, J. Phys. Chem. Solids 60 (1999), pp. 189–193.
[16] P.R. Guagliardo, E.R. Vance, Z. Zhang, J. Davis, J.F. Williams, and S.N. Samarin, *Positron annihilation lifetime studies of Nb-doped TiO_2, SnO_2, and ZrO_2*, J. Am Ceram. Soc. 95 (2012), pp. 1727–1731.
[17] J. Čížek, O. Melikhova, I. Procházka, J. Kuriplach, R. Kužel, G. Brauer, W. Anw, T.E. Konstantinova, and I.A. Danilenko, *Defect studies of nanocrystalline zirconia powders and sintered ceramics* Phys. Rev. B 81 (2010), pp. 024116:1–19.
[18] M.A. Ponce, C. Macchi, F. Schipani, C.M. Aldao, and A. Somoza, *Mild degradation processes in ZnO-based varistors: The role of Zn vacancies*, Phil. Mag. 95 (2015), pp. 730–743.
[19] C. Buono, D.A. Mirabella, and C.M. Aldao, *Sensitivity of metal oxide gas sensors to non-parabolic intergranular barriers*. Sens Actuators B, Chem. 246 (2017), pp. 1025–1029.
[20] P.M. Desimone, C.G. Díaz, J.P. Tomba, C.M. Aldao, and M.A. Ponce, *Reversible metallization of SnO_2 films under hydrogen and oxygen containing atmospheres*, J. Mater. Sci. 51 (2016), pp. 4451–4461.
[21] F. Schipani, M.A. Ponce, E. Joanni, F.J. Williams, and C.M. Aldao, *Study of the oxygen vacancies changes in SnO_2 polycrystalline thick films using impedance and photoemission spectroscopies*, J. Appl. Phys. 116 (2014), pp. 194502:1–8.
[22] I.I.C.f.D. Data, Powder Diffraction File Database, EEUU, Newtown Square, 1998.
[23] C.M. Aldao, F. Schipani, M.A. Ponce, E. Joanni, and F.J. Williams, *Conductivity in SnO_2 polycrystalline thick film gas sensors: Tunneling electron transport and oxygen diffusion*, Sens. Actuators B, Chem. 193 (2014), pp. 428–433.
[24] P. Kirkegaard, N.J. Pedersen, and M. Eldrup, PATFIT-88 program, Tech. Rep. M-2740, Risoe National Laboratory, Roskilde, Denmark, 1989.
[25] K. MacKenzie, *Experimental methods of annihilation time and energy spectrometry*, in *Positron Solid-State Physics, International School of Physics «Enrico Fermi», Course LXXXIII*, W. Brandt and A. Dupasquier, eds., North-Holland, Amsterdam, 1983, pp. 196–264.

[26] T.G.G. Maffeïs, G.T. Owen, C. Malagù, G. Martinelli, M.K. Kennedy, F.E. Kruis, and S.P. Wilks, *Direct evidence of the dependence of surface state density on the size of SnO_2 nanoparticles observed by scanning tunnelling spectroscopy*, Surf. Sci. 550 (2004), pp. 21–25.

[27] C. Malagù, G. Martinelli, M.A. Ponce, and C.M. Aldao, *Unpinning of the Fermi level and tunneling in metal oxide semiconductors*, Appl. Phys. Lett. 92 (2008), pp. 162104: 1–3.

[28] T. Pagnier, M. Boulova, N. Sergent, P. Bouvier, and G. Lucazeau, *Nanopowders and nanostructured oxides: Phase transitions and surface reactivity*, J. Raman Spectrosc. 38 (2007), pp. 756–761.

[29] J.X. Wang, D.F. Liu, X.Q. Yan, H.J. Yuan, L.J. Ci, Z.P. Zhou, Y. Gao, L. Song, L.F. Liu, W.Y. Zhou, G. Wang, and S.S. Xie, *Growth of SnO_2 nanowires with uniform branched structures*, Solid State Commun. 130 (2004), pp. 89–94.

[30] M. Ristić, M. Ivanda, S. Popović, and S. Musić, *Dependence of nanocrystalline SnO_2 particle size on synthesis route*, J. Non-Cryst. Solids 303 (2002), pp. 270–280.

[31] S.H. Sun, G.W. Meng, G.X. Zhang, T. Gao, B.Y. Geng, L.D. Zhang, and J. Zuo, *Raman scattering study of rutile SnO_2 nanobelts synthesized by thermal evaporation of Sn powders*, Chem. Phys. Lett. 376 (2003), pp. 103–107.

[32] O.M. Berengue, R.A. Simon, A.J. Chiquito, C.J. Dalmaschio, E.R. Leite, H.A. Guerreiro, and F.E.G. Guimarães, *Semiconducting Sn_3O_4 nanobelts: Growth and electronic structure* J. Appl. Phys. 107 (2010), pp. 033717: 1–4

[33] K.K. Nanda and S.N. Sahu, *Study of CdS nanocrystallites by AFM and Raman scattering spectroscopy*, Appl. Surf. Sci. 119 (1997), pp. 50–54.

[34] S. Ushioda, A. Aziza, J.B. Valdez, and G. Mattei, *Effects of surface roughness on surface polaritons*, Phys. Rev. B 19 (1979), pp. 4012–4019.

[35] R. Fukasawa, M. Wakaki, K. Ohta, and H. Okumura, *Raman scattering determination of free carrier concentration and surface depletion layer in (100) p-GaAs grown by molecular-beam epitaxy*, Jpn. J. Appl. Phys. 25 (1986), pp. 652–653.

[36] G. Abstreiter, E. Bauser, A. Fisher, and K. Ploog, *Raman spectroscopy – A versatile tool for characterization of thin films and heterostructures of GaAs and $AlxGa_{1\_}xAs$*, Appl. Phys. 16 (1978), pp. 345–352.

[37] J. Zuo, C. Xu, X. Liu, and C. Wang, *Study of the Raman spectrum of nanometer SnO_2*, J. Appl. Phys. 75 (1994), pp. 1835–1836.

[38] J. Xu, Y. Li, H. Huang, Y. Zhu, Z. Wang, Z. Xie, X. Wang, D. Chen, and G. Shen, *Synthesis, characterizations and improved gas-sensing performance of SnO_2 nanospike arrays*, J. Mater. Chem. 21 (2011), pp. 19086–19092.

[39] L.M. Sharygin and S.M. Vovk, *Raman spectroscopy studies of structural changes in hydrated titanium and tin dioxide gels under drying*, J. Appl. Spectrosc. 64 (1997), pp. 283–286.

[40] P. Hautojärvi (ed.), *Positrons in Solids. Vol. 12. Topics in Current Physics*, Springer, Berlin Heidelberg, 1979.

[41] H.E. Schaefer, R. Würschum, R. Birringer, and H. Gleiter, *Structure of nanometer-sized polycrystalline iron investigated by positron lifetime spectroscopy*, Phys. Rev. B 38 (1988), pp. 9545–9554.

[42] R. Checchetto, N. Bazzanella, A. Kale, A. Miotello, S. Mariazzi, R.S. Brusa, P. Mengucci, C. Macchi, A. Somoza, W. Egger, and L. Ravelli, *Enhanced kinetics of hydride-metal phase transition in magnesium by vacancy clustering*, Phys. Rev. B 84 (2011), pp. 054115: 1–7.

[43] C. Macchi, C. Maurizio, R. Checchetto, S. Mariazzi, L. Ravelli, W. Egger, P. Mengucci, N. Bazzanella, A. Miotello, A. Somoza, and R.S. Brusa, *Niobium aggregation and vacancylike defect evolution in nanostructured Nb-doped Mg: Their role in the kinetics of the hydride-to-metal phase transformation* Phys. Rev. B 85 (2012), pp. 214117: 1–19

[44] A. Dupasquier, R. Romero, and A. Somoza, *Positron trapping at grain boundaries*, Phys. Rev. B 48 (1993), pp. 9235–9245.

[45] M.A. Ponce, C. Malagù, M.C. Carotta, G. Martinelli, and C.M. Aldao, *Gas indiffusion contribution to impedance in tin oxide thick films*, J. Appl. Phys. 104 (2008), pp.054907: 1–5.
[46] C. Malagù, M.C. Carotta, A. Giberti, V. Guidi, G. Martinelli, M.A. Ponce, M.S. Castro, and C.M. Aldao, *Two mechanisms of conduction in polycrystalline SnO_2*, Sens. Actuators B Chem. 136 (2009), pp. 230–234.
[47] R. Savu, M.A. Ponce, E. Joanni, P.R. Bueno, M.S. Castro, M. Cilense, E. Longo, and J.A. Varela, *Grain size effect on the electrical response of SnO_2 thin and thick film gas sensors*, Mater. Res. 12 (2009), pp. 85–89.
[48] J.H.C. van Hooff and J.F. van Helden, *Formation of peroxo radicals on tin dioxide*, J. Catal. 8 (1967), pp. 199–200.
[49] J.H.C. van Hooff, *Formation of paramagnetic surface species during the oxidation of nonstoichiometric TiO_2(A), SnO_2, and ZnO*, J. Catal. 11 (1968), pp. 277–279.
[50] P. Meriaudeau, C. Naccache, and A. Tench, *Paramagnetic oxygen species adsorbed on reduced SnO_2*, J. Catal. 21 (1971), pp. 208–211.
[51] C. Hauser, *Considerations on oxygen paramagnetic centres adsorbed on TiO_2 and SnO_2*, Chem. Phys. Lett. 18 (1973), pp. 205–208.
[52] Y. Mizokawa and S. Nakamura, *ESR study of adsorbed oxygen on tin dioxide*, Oyo Buturi. 46 (1977), pp. 580–584. (in Japanese).
[53] S.C. Chang, *Oxygen chemisorption on tin oxide: Correlation between electrical conductivity and EPR measurements*, J. Vac. Sci. Technol. 17 (1980), pp. 366–369.
[54] C. Malagù, A. Giberti, S. Morandi, and C.M. Aldao, *Electrical and spectroscopic analysis in nanostructured SnO_2: 'Long-term' resistance drift is due to in-diffusion*, J. Appl. Phys. 110(093711) (2011), pp. 1–4.
[55] B. Kamp, R. Merkle, R. Lauck, and J. Maier, *Chemical diffusion of oxygen in tin dioxide: Effects of dopants and oxygen partial pressure*, J. Solid State Chem. 178 (2005), pp. 3027–3039.
[56] M.A. Ponce, M.S. Castro, and C.M. Aldao, *Capacitance and resistance measurements of SnO_2 thick-films*, J. Mater. Sci: Mater Electron 20 (2009), pp. 25–32.
[57] A.Z. Sadek, S. Choopun, W. Wlodarski, S.J. Ippolito, and K. Kalantar-zadeh, *Characterization of ZnO nanobelt-based gas sensor for H_2, NO_2, and hydrocarbon*, Sens. IEEE Sens. J. 7 (2007), pp. 919–924.
[58] P.M. Desimone, C.G. Díaz, J.P. Tomba, C.M. Aldao, and M.A. Ponce, *Reversible metallization of SnO_2 films under hydrogen and oxygen containing atmospheres*, J. Mater. Sci. 51 (2016), pp. 4451–4461.
[59] F. Schipani, D.R. Miller, M.A. Ponce, C.M. Aldao, S.A. Akbar, and P.A. Morris, *Electrical characterization of semiconductor oxide-based gas sensors using impedance spectroscopy: A review*, Rev. Adv. Sci. Eng. 5 (2016), pp. 86–105.
[60] N. Barsan, D. Koziej, and U. Weimar, *Metal oxide-based gas sensor research: How to?*, Sens. Actuators B 121 (2007), pp. 18–35.
[61] S. Lany and A. Zunger, *Dopability, intrinsic conductivity, and nonstoichiometry of transparent conducting oxides*, Phys. Rev. Lett. 98(045501) (2007), pp. 1–4.
[62] S.B. Zhang, S.H. Wei, and A. Zunger, *A phenomenological model for systematization and prediction of doping limits in II–VI and I-III–VI_2 compounds*, J. Appl. Phys. 83 (1998), pp. 3192–3196.